Volume 18, No 2 | International Journal of Radiation Research, April 2020

Investigation of irregular radiation field-based proton therapy using conformal dose layer stacking method

W. Shao[1,3], X. Tang[1,2*], C. Geng[1], D. Shu[1], C. Gong[1], X. Zhang[1], F. Guan[4]

[1]*Department of Nuclear Science and Engineering, Nanjing University of Aeronautics and Astronautics, Nanjing, China*
[2]*Collaborative Innovation Center of Radiation Medicine of Jiangsu Higher Education Institutions, Nanjing, China*
[3]*Department of Radiation Physics, Harbin Medical University Cancer Hospital, Harbin, China*
[4]*Department of Radiation Physics, The University of Texas MD Anderson Cancer Center, Houston, USA*

► ***Original article***

Corresponding authors:
Xiaobin Tang, Ph.D.,
E-mail:
tangxiaobin@nuaa.edu.cn

Revised: June 2019
Accepted: July 2019
Int. J. Radiat. Res., April 2020; 18(2): 295-306
DOI: 10.18869/acadpub.ijrr.18.2.295

ABSTRACT

Background: Dose modulation is a key factor in practical proton therapy. This study investigates the dose modulation methodology of irregular radiation field (IRF)-based proton therapy using forward radiation treatment planning and conformal dose layer stacking (CDLS) methods. ***Materials and Methods:*** The geometric configuration of a virtual multi-leaf system was constructed to generate IRFs during Monte Carlo simulations. Two patient geometries—lymphatic metastasis and brain tumors—were configured to investigate the dosimetric feasibility and applications of IRF-based proton therapy in ideal patient anatomies. The investigated tumors were divided into slices perpendicular to proton beam axis. Segments were designed to be conformal to the profiles of these tumor slices. Conformal dose layers were produced by modulating the proton intensities and energies of the predesigned segments. Then, these dose layers were stacked throughout the tumors to obtain sufficient and conformal tumor doses. ***Results:*** From the proposed IRF-based proton therapy, tumors with 4-7 cm extents along the depth direction could be treated with fewer than 10 segments. The lymphatic metastasis and brain tumors were sufficiently covered by 95% dose lines, while appropriate distal and proximal dose conformities were achieved. The maximum tumor doses did not exceed 110%. ***Conclusions:*** Theoretically, the proposed IRF-based proton therapy using forward planning and CDLS methods is feasible from the viewpoint of dosimetry. This study can serve as a foundation for future investigations of potential proton therapy methods based on fast conformal dose layer stacking using radiation fields with irregular shapes.

Keywords: *Proton therapy, dose modulation, radiation field, irregular shape, forward planning.*

INTRODUCTION

Proton therapy is an effective therapeutic method that is suitable for treating patients with malignant tumors [1-4]. In proton therapy, high dose regions can be located inside tumors based on the physical properties of Bragg peak formation in human tissues [5,6]. The absorbed doses beyond tumors can be controlled to a low level. Hence, damage to normal tissues is reduced, especially in the tissues distal to malignant tumors [7-10].

Conformal proton therapy (CPT), which is a type of passive-scattering proton therapy based on patient-specific apertures and range compensators, is a commonly used proton therapy method [11-13]. For this method, prescribed dose profiles distal to tumors can be adjusted to conform to tumor outlines [14]. However, proximal dose conformities of tumors are sacrificed owing to the lack of proton intensity modulation during radiation treatment

[DOI: 10.18869/acadpub.ijrr.18.2.295]

planning. This leads to extra proton irradiation to normal tissues proximal to tumors and increases the probability of radiotherapy complications. Scanned beam-based intensity-modulated proton therapy (IMPT) has been developed and applied to enhance the conformities between prescribed dose profiles and tumor contours. For this proton therapy modality, dose spots generated around Bragg peaks of narrow proton beams are utilized to scan throughout tumors in a point-by-point manner. Thus, good conformities between tumor profiles and prescribed dose lines are realized, and excellent performance is achieved in treating static tumors with complicated geometric configurations [15-18]. However, in scanned beam-based IMPT, only one "spot" inside a tumor is irradiated at any given time. Theoretically, the dose delivery efficiency of scanned beam-based IMPT could be relatively limited owing to the point-by-point treatment pattern for a specified dose rate. Considering the limitations of CPT and IMPT, it is necessary to investigate possible dose modulation and delivery methods by which conformal doses can be delivered to tumors with high delivery efficiency.

In this paper, we propose a novel dose modulation method inspired by Carbon 3D printing [19]. Unlike traditional 3D printing with a point-by-point printing pattern, Carbon 3D offers the beneficial ability of instantaneous layer-by-layer printing. For traditional 3D printing technology, only one point is printed at any given time. With the Carbon 3D printing technology, a whole conformal layer can be instantaneously printed in an instant. Thus, the efficiency of Carbon 3D printing is 25-100 times higher than that of traditional 3D printing technologies. It is expected that this kind of instantaneous layer-by-layer printing strategy can be applied to dose "printing" in proton therapy, although there is a physical difference between the material stacking of Carbon 3D printing technology and the energy layer stacking of proton therapy. Hence, this study investigated the proton therapy methodology by which an instantaneous layer-by-layer "dose printing" pattern can be adopted rather than the point-by-point pattern used by scanned beam-based IMPT.

In this study, the geometric configuration of a virtual multi-leaf collimation (MLC) system was adopted to generate proton radiation fields with irregular shapes. Two patient geometries—lymphatic metastasis and brain tumors—were each constructed to investigate whether the proposed IRF-based proton therapy can be applied to human anatomic structures in a tentative manner. First, the investigated tumors were divided into thin tumor slices perpendicular to the proton beam axis. Secondly, the segments conformal to the profiles of these tumor slices were designed based on the virtual MLC system. Thirdly, conformal dose layers were produced for each of the tumor slices by modulating the proton intensities and energies of each predesigned segment. Next, the conformal dose layers were stacked throughout the tumors to sufficiently cover them. Dose distributions in the investigated tumors were assessed for each of the tumor cases. To some extent, this study could elucidate the possibilities for a fast conformal-dose-layer stacking technology based on radiation fields with irregular shapes in proton therapy.

MATERIALS AND METHODS

Monte Carlo particle transport codes have been widely accepted and applied in the field of medical physics [20-27]. The GEANT4 Monte Carlo toolkit (version 4.10.1.p02) was used to perform the dose calculation tasks in this study. In this section, an ideal water phantom with a centrally located tumor was adopted to demonstrate the methods used to produce uniform doses conformal to tumor profiles using the forward treatment planning and conformal dose layer stacking (CDLS) methods. A virtual MLC with a 5 -mm leaf width was configured to generate IRFs. Three procedures for the proposed IRF-based proton therapy were conceived, and they are described as follows:

- "Chop" the tumor into tumor slices.
- Design segment shapes conformal to the profiles of the "chopped" tumor slices.

[DOI: 10.18869/acadpub.ijrr.18.2.295]

- Produce uniform dose layers conformal to the profiles of the tumor slices.

Moreover, possible solutions with the potential ability to drastically reduce the number of segments and segment shape switches are also proposed in this section.

Chop the tumor into thin tumor slices

As illustrated in figure 1, a spherical tumor with a 10 cm diameter was centrally placed inside the virtual water phantom. Then, it was "chopped" into ten tumor slices with 1 cm thicknesses. Proton beams were incident on the ideal phantom perpendicular to the left phantom surface. Collimated by the virtual MLC, the proton beams with energies E_1-E_{10} formed Bragg peaks and produced conformal dose layers inside each tumor slice. In figure 2, the tumor chopping process is illustrated in a three-dimensional pattern. As illustrated in figures 2(a) and 2(b), the tumor was divided into ten slices perpendicular to the Z-axis after the chopping process. Then, as shown in figure 2(c), these tumor slices were numbered and respectively exhibited in a two-dimensional pattern.

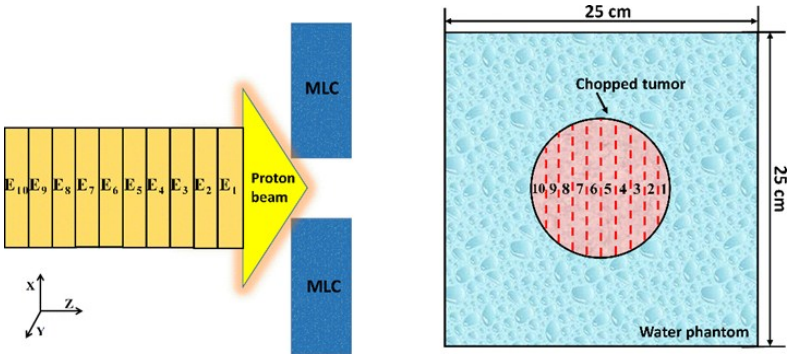

Figure 1. Geometry configuration for the investigation of conformal dose layer production.

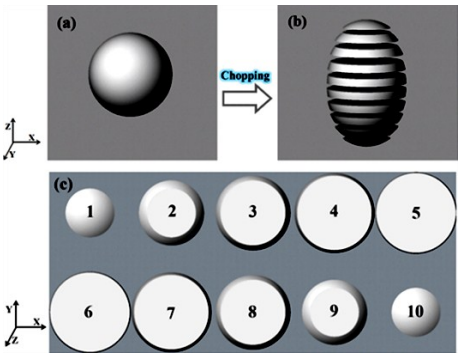

Figure 2. Illustration of the tumor chopping process: **(a)** tumor diagram before the chopping process; **(b)** the tumor diagram after chopping process; **(c)** exhibitions for each numbered tumor slice.

Design segment shapes conformal to the profiles of the "chopped" tumor slices

In this section, tumor slices 1-4 are taken as examples to briefly demonstrate the method for designing segment shapes conformal to the profiles of the "chopped" tumor slices. First, tumor slices 1-4 were divided into several irradiated parts, as illustrated in figure 3. The irradiated areas of tumor slices 1-4 (S_1-S_4) can be expressed by Eqs. 1-4:

$$S_1 = S_{slice1} \quad (1)$$

$$S_2 = S_{slice1} \cup (\overline{S_{slice1}} \cap S_{slice2}) \quad (2)$$

$$S_3 = S_{slice1} \cup (\overline{S_{slice1}} \cap S_{slice2}) \cup (\overline{S_{slice2}} \cap S_{slice3}) \quad (3)$$

$$S_4 = S_{slice1} \cup (\overline{S_{slice1}} \cap S_{slice2}) \cup (\overline{S_{slice2}} \cap S_{slice3}) \cup (\overline{S_{slice3}} \cap S_{slice4}) \quad (4)$$

Where; S_{slice1}- S_{slice4} denote the projection areas of tumor slices 1-4 on the X-Y plane, respectively. As shown by Eqs. 1-4, S_1, S_2, S_3, and S_4 were respectively classified into 1, 2, 3, and 4 parts, which are clearly indicated by the red dotted lines. This kind of classification aimed to modulate proton intensities within the divided parts and achieve uniformly distributed doses in the tumor slices. After that, segment shapes conformal to the profiles of these parts should be obtained for tumor slices 1-4. Seven segment shapes (see figures 4(a)-4(g)) were designed and selectively allocated to tumor slices 1-4. The segment shape information for each tumor slice is listed in table 1. Segment shape 1 was designed to be conformal to the profile of tumor slice 1. For tumor slice 2, segment shape 1 was re-allocated to part 1. Segment shapes 2 and 3 were designed for part 2. For tumor slice 3, segment shape 1 was re-allocated to part 1, and

[DOI: 10.18869/acadpub.ijrr.18.2.295]

segment shapes 2 and 3 were re-allocated to part 2. Segment shapes 4 and 5 were designed for part 3. For tumor slice 4, segment shape 1 was re-allocated to part 1, segment shapes 2 and 3 to part 2, and segment shapes 4 and 5 to part 3. Segment shapes 6 and 7 were designed for part 4. For tumor slices 5-10, correspondent segment shapes were designed and allocated based on a similar designing method to that for tumor slices 1-4.

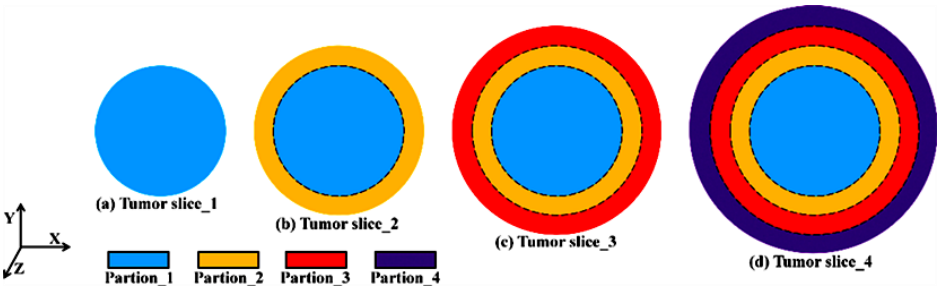

Figure 3. Illustration of the segmentation process for tumor slices 1-4.

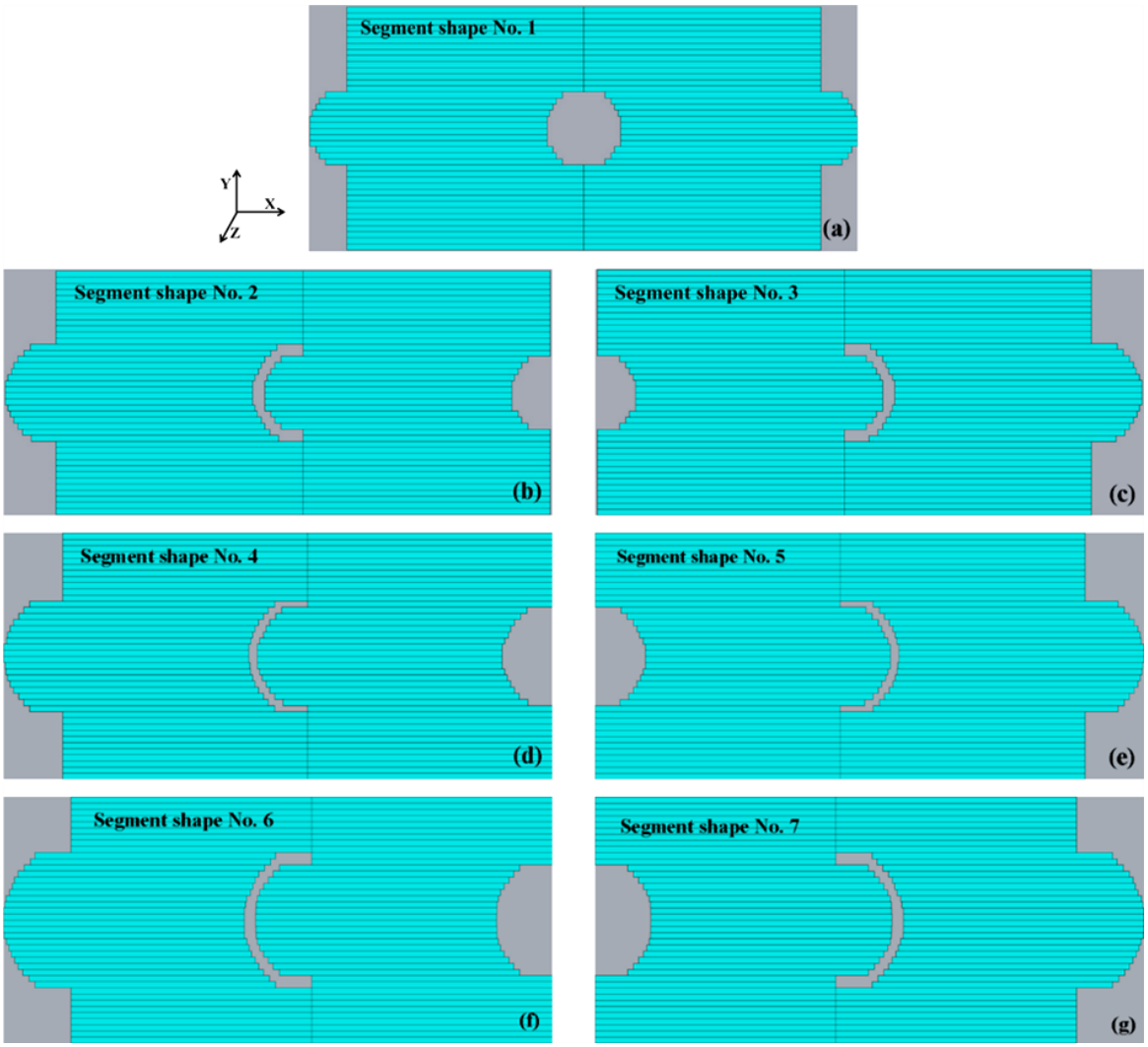

Figure 4. Illustration of the designed segment shapes with serial numbers 1-7.

[DOI: 10.18869/acadpub.ijrr.18.2.295]

Table 1. Information of the segment shape constitutions for tumor slices 1-10.

Tumor slice	Segment shape	Tumor slice	Segment shape
No. 1	No. 1	No. 6	No. 1-7
No. 2	No. 1-3	No. 7	No. 1-7
No. 3	No. 1-5	No. 8	No. 1-5
No. 4	No. 1-7	No. 9	No. 1-3
No. 5	No. 1-7	No. 10	No. 1

Produce dose layers conformal to the profiles of the "chopped" tumor slices

Collimated by the predesigned segment shapes, proton beams with energies E_1-E_{10} can respectively produce "dose fragments" (see figures 5(a)-5(g)) inside tumor slices 1-10. Information on the required "dose fragments" of tumor slices 1-10 is listed in table 2. As shown in figure 5, the profiles of "dose fragments" 1-7 were almost conformal to the contours of segment shapes 1-7. By modulating the weight of these dose fragments, uniformly distributed doses (see figures 6(a)-6(j)) conformal to the profiles of tumor slices 1-10 could be obtained. By stacking these uniform dose layers (see figures 6(a)-6(j)), uniform dose distributions conformal to the profile of the investigated tumor could be derived.

As shown in figure 7(a), prescribed doses are delivered to the tumor in a layer-by-layer pattern. This type of dose delivery required at least 37 segment shape switches. Conventionally, segment shape switches are accomplished via the mechanical movement of heavy metal multi-leaves driven by electric motors. Frequent segment shape switches could greatly decrease dose delivery efficiency. Thus, we conceived the dose delivery pattern illustrated in figure 7(b).

As exhibited in figure 7(b), dose delivery is realized in a segment shape-by-segment shape pattern. The segments required by delivering sufficient doses to the tumor were classified into seven sequences based on the segment shapes indicated by the red dotted lines. Hence, each of the seven sequences can be deemed as an "integrated" segment with identical segment shapes and multiple beam energies. From this viewpoint, only seven segments were required to treat the spherical tumor. Compared with the layer-by-layer delivery pattern, the number of segment shape switches was reduced from 37 to 6 (a factor of more than 6). Dose delivery efficiency was thus enhanced. This kind of dose delivery was more appropriate for pursuing high delivery efficiency, and it is recommended for utilization in the proposed IRF-based proton therapy.

The main purpose of this section was to briefly demonstrate the methods for producing uniform dose layers conformal to the tumor slice profiles for the proposed IRF-based proton therapy, not to detail the dose calculation processes and calculated doses. Hence, detailed tumor dose exhibitions were not included in this section. Detailed dose calculations were performed based on lymphatic metastasis and brain tumors in the next section. During the demonstration of the dose producing method, we used the notations of E_1-E_{10} (see table 2) instead of specific beam energy values because these denotations are more representative than specific energy values.

Table 2. Beam energy and dose fragment constitution information for tumor slices 1-10.

Dose layer	Tumor slice	Beam energy	Dose fragment
No. 1	No. 1	E_1	No. 1
No. 2	No. 2	E_2	No. 1-3
No. 3	No. 3	E_3	No. 1-5
No. 4	No. 4	E_4	No. 1-7
No. 5	No. 5	E_5	No. 1-7
No. 6	No. 6	E_6	No. 1-7
No. 7	No. 7	E_7	No. 1-7
No. 8	No. 8	E_8	No. 1-5
No. 9	No. 9	E_9	No. 1-3
No. 10	No. 10	E_{10}	No. 1

[DOI: 10.18869/acadpub.ijrr.18.2.295]

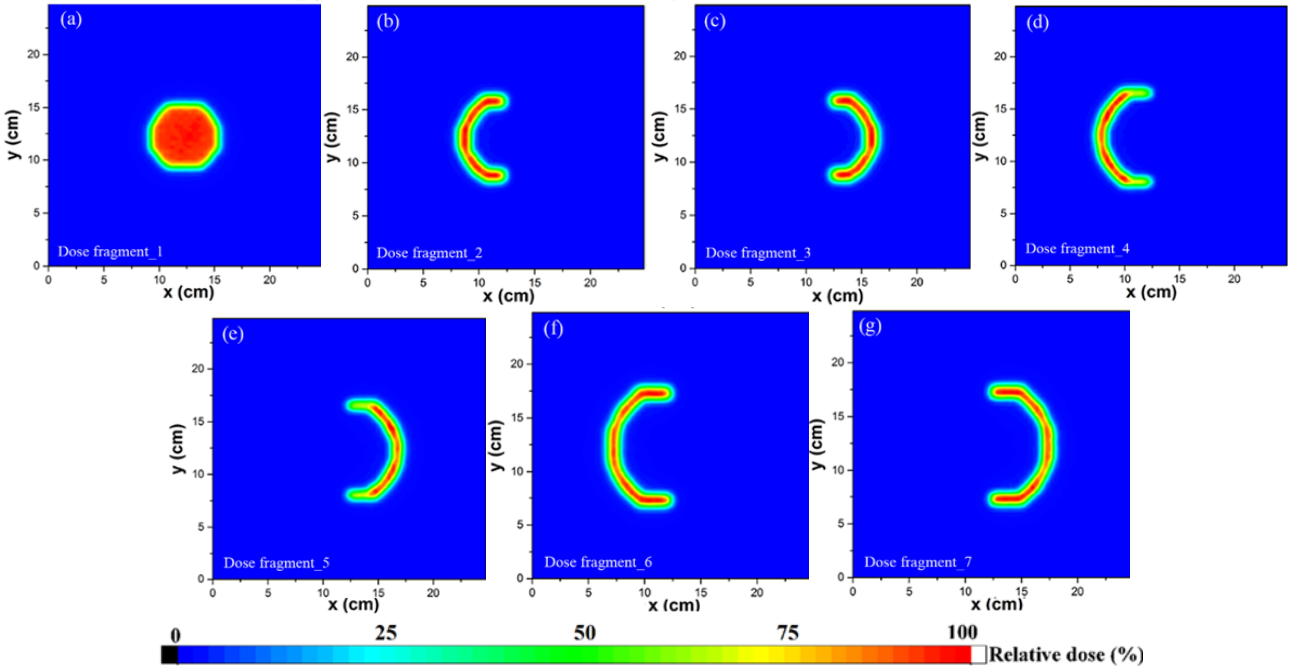

Figure 5. Selective illustrations of the dose profiles for segment shapes 1-7 crossing the fourth tumor slice.

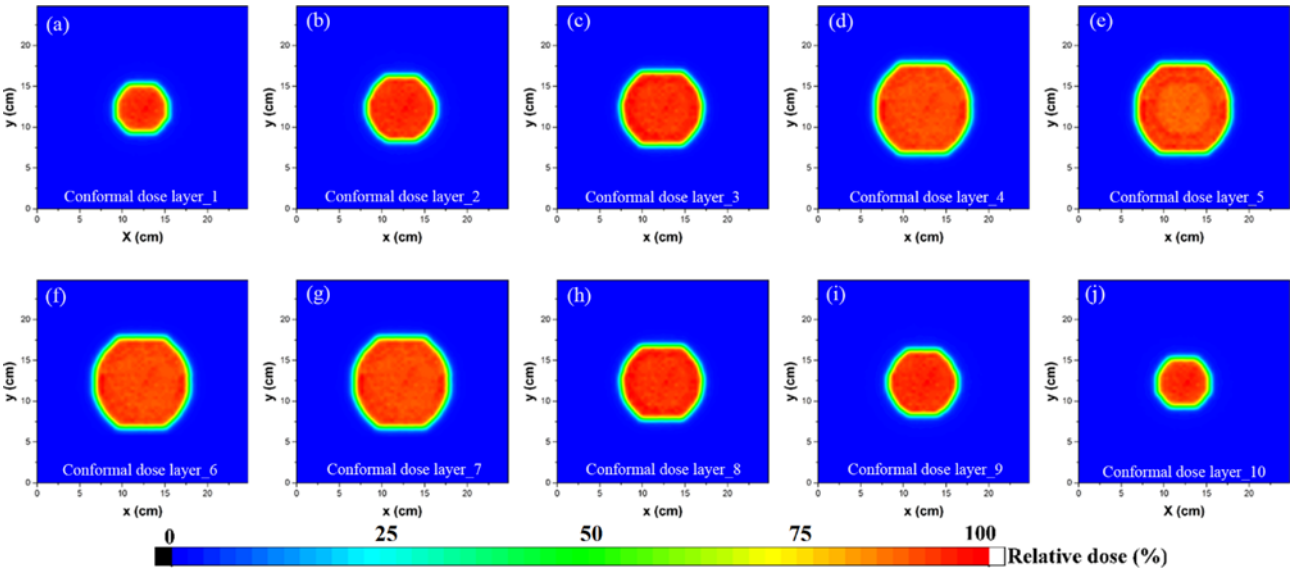

Figure 6. Illustration of conformal dose layers corresponding to tumor slices 1-10.

[DOI: 10.18869/acadpub.ijrr.18.2.295]

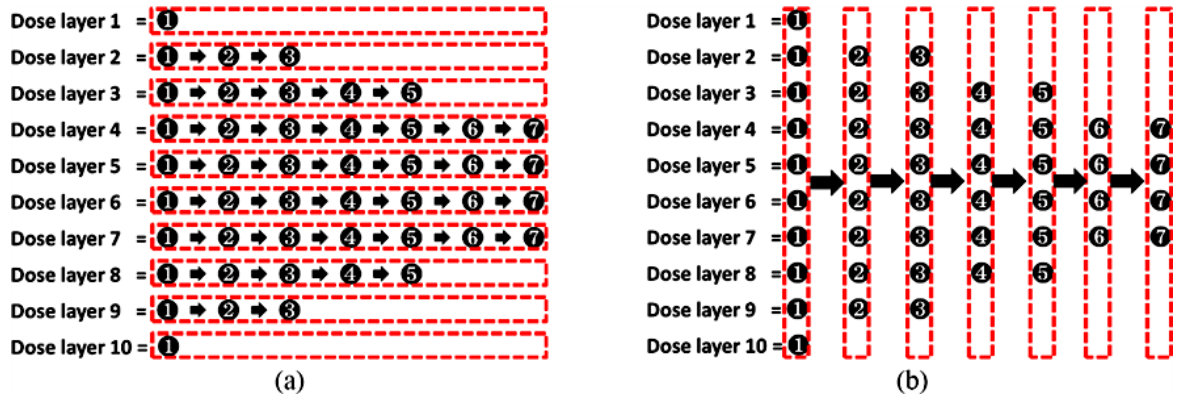

Figure 7. Possible dose delivery patterns: **(a)** layer-by-layer; **(b)** segment shape-by-segment shape. Appropriate dose delivery patterns have the potential to enhance treatment efficiency by reducing the number of segment shape switches. Figure 7 demonstrates two possible dose delivery patterns that were conceived for the proposed IRF-based proton therapy. In figure 7, each equation lists the serial number of the respective segment shapes required by dose layers 1-10. The clusters of serial numbers surrounded by the red dotted lines denote the possible segment shape sequences used to deliver doses to the tumor. The black arrows represent segment shape switches, and the number of black arrows is equal to the number of segment shape switches.

RESULTS

In this section, two human geometric configurations—lymphatic metastasis and brain tumors—were each employed to investigate the potential applications of forwarding IRF-based proton therapy in a tentative manner using the CDLS method. The lymphatic metastasis and brain tumors were respectively chopped into 10 and 8 tumor slices of 5 mm in thickness. Conformal segment shapes were designed for the two investigated tumors based on the designing mechanism proposed in the previous section. The dose distributions inside the two investigated tumors are illustrated in figures 8 and 9. In these figures, the white dotted lines outline the profiles of the investigated tumors. The black solid lines surrounding the tumor contours represent 95% relative dose lines.

Abdominal configuration with the lymphatic metastasis tumor

For the lymphatic metastasis tumor case, five segment shapes and five "integrated" segments were designed to obtain sufficient tumor doses and appropriate dose conformity following the design mechanism proposed in the previous section. The proton energies of these "integrated" segments ranged from 110 to 130 MeV. Proton beams were incident on the patient's body along the negative Z-axis, as shown in figure 8(a), and the angle between the proton beam axis and the Z-axis was 180º. The interactions between the proton beams collimated by the predesigned segments and the ideal abdominal phantom were simulated using GEANT4. The dose distributions in the abdominal phantom were calculated, and they are exhibited in figures 8(a) and (b).

As illustrated in figure 8(a), the lymphatic metastasis tumor was sufficiently covered by the 95% relative dose line in the X-Z plane, and the maximum relative dose was less than 110%. The profile of the 95% dose line was almost conformal to the contour of the lymphatic metastasis tumor, especially in the region proximal to the tumor. Compared with traditional passive scattering methods, the improvement of proximal dose conformity can significantly reduce the doses received by vital organs proximal to the tumor. This kind of dose conformity improvement was beneficial to the dose reduction of the small intestine, which is proximal to the lymphatic metastasis tumor. Thus, radiotherapy complications related to the small intestine can be mitigated to some extent. As plotted in figure 8(b), the profile of the 95% relative dose line fits well with the tumor contour, and relative doses larger than 110% were not observed in the plane crossing the fourth tumor slice. Overall, satisfiable distal dose

[DOI: 10.18869/acadpub.ijrr.18.2.295]

conformities were achieved using less than 10 "integrated" segments, while appropriate proximal dose conformities were realized through the proposed IRF-based proton therapy.

Head configuration with the brain tumor

For the brain tumor case, we designed seven segment shapes and seven "integrated" segments following the design mechanism proposed in the previous section. The energies of the proton beams corresponding to these "integrated" segments ranged from 80 to 105 MeV. Proton beams were incident on the patient body along the positive Z-axis, as plotted in figure 9(a), and the angle between the proton beam axis and the Z-axis was approximately 0°. The simulations for the interactions between protons and the ideal head phantom were performed using GEANT4. The dose distributions achieved by the proposed IRF-based proton therapy in the head phantom are shown in figure 9.

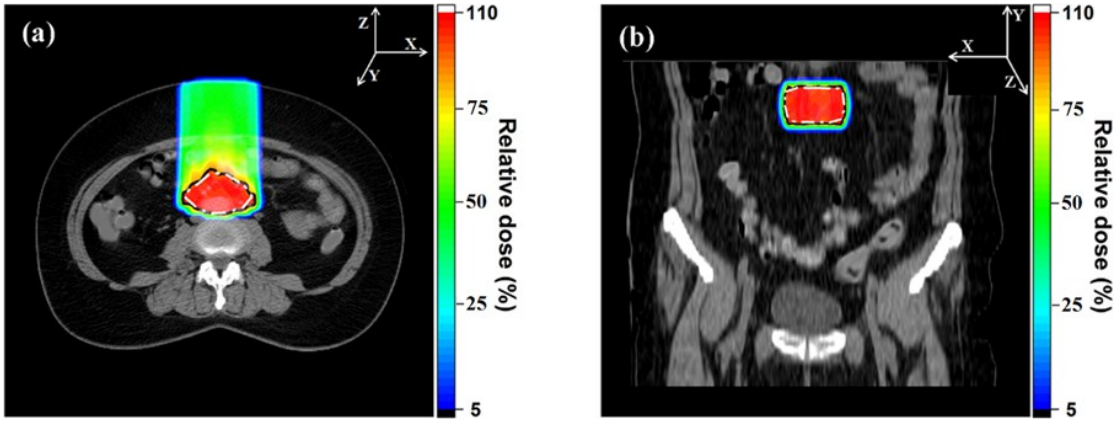

Figure 8. Relative dose distributions obtained by forwarding IRF-based proton therapy for the lymphatic metastasis tumor case: **(a)** in the X-Z plane; **(b)** in the X-Y plane crossing the fourth tumor slice.

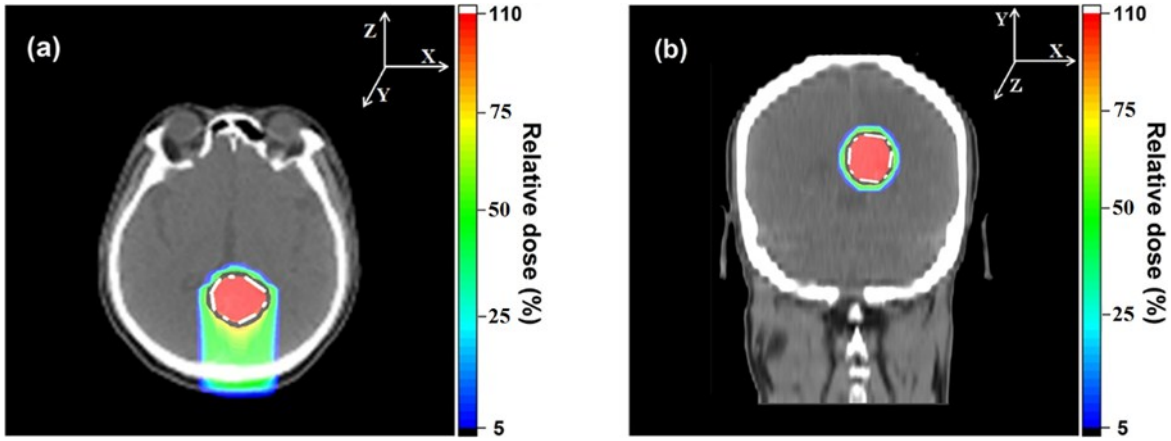

Figure 9. Relative dose distributions obtained by forwarding IRF-based proton therapy for the brain tumor case: **(a)** in the X-Z plane and **(b)** in the X-Y plane crossing the fourth tumor slice

DISCUSSION

For IRF-based proton therapy, the dose deposition of a proton beam with specified energy is mainly confined within a specified tumor slice around the Bragg peak. Hence, dose modulation is necessary for every tumor slice, and a sizable number of segments could be required by IRF-based proton therapy via inverse treatment planning. In an existing investigation, it was revealed that almost hundreds of segments are required to treat a

[DOI: 10.18869/acadpub.ijrr.18.2.295]

tumor with a 10 cm extent in the depth direction for an inverse treatment plan [28]. Owing to frequent segment shape switches, treatment time could be a problematic issue for practical applications of IRF-based proton therapy via inverse treatment planning. As described in the Materials and Methods section, we conceived three effective solutions for reducing the number of segments required by IRF-based proton therapy, which are as follows:

- Rather than inverse radiation treatment planning, forward planning was employed to enhance control over segment shape design because forward planning is not restricted by inverse optimization algorithms.
- Segment shapes were shared and reused among different tumor slices to reduce the numbers of segment shapes required.
- The segments were classified with identical segment shapes and different energies into "integrated" segments to decrease the frequency of segment shape switches.

The applications of the scanned beam-based IMPT in treating moving tumors are largely limited by a so-called interplay effect caused by tumor motion [29]. However, four-dimensional CT scanning only provides a snapshot in time and cannot necessarily exhibit 4D patient geometries during a treatment fraction [30]. Most existing studies recommend prediction of time-related dose distributions through treatment planning based on 4D CT data and offsetting possible dose deteriorations caused by tumor motion via rescanning [31-36]. Thus, it is still necessary to explore potential technical solutions for accurate dose delivery to moving tumors.

Conventionally, irregular photon beams are widely applied in intensity modulated radiation therapy (IMRT) [37-42]. With the aid of active breath control (ABC) technology, IRF-based IMRT has the potential to deliver conformal doses to moving targets to some extent. For this kind of treatment strategy, moving tumors are deemed as static tumors during the breath hold status. Hence, accurate dose delivery can be accomplished during the breath hold status while tumors are almost static. To duplicate the beneficial strategies of ABC-IMRT collaboration in moving tumor treatments, segments quantities required by IRF-based proton therapy should be insensitively decreased and controlled to a relatively acceptable level. The IRF-based proton therapy proposed in this paper can treat tumors with less than 10 segments, which is comparable to the segment quantities used in an IMRT treatment plan. From this viewpoint, the methods and mechanism described in this paper could instigate potential collaboration of ABC and IRF-based proton therapy for the accurate treatment of moving tumors to some extent.

In this study, simple-shaped lymphatic metastasis and brain tumors were used to investigate the dosimetric feasibility of the proposed IRF-based proton therapy in human anatomies. The original motivation of the proposed IRF-based proton therapy was not to compete with scanned beam-based IMPT in terms of dose uniformity and conformity but to theoretically provide the potential to enhance dose delivery efficiency under specified dose rates. Thus, reducing segment quantities and segment switches are the most important tasks for the proposed forward IRF-based proton therapy. However, complicated geometries will increase the numbers of segments required for forwarding radiation treatment plans. This kind of adverse influence clearly opposes the essential motivation of this study. Considering the above descriptions, we do not recommend the proposed IRF-based proton therapy for treating tumors with complicated geometries. The proposed IRF-based proton therapy should mainly be used to introduce higher treatment efficiency while dealing with relatively large tumors with relatively simple geometries. Beneficial dosimetric investigations are still valuable for tumors with relatively complicated geometries if medical physicists and radiation oncologists are interested in the proposed IRF-based proton therapy. For this kind of research, the tradeoff between the numbers of "integrated" segments and tumor dose conformities is a key factor that should be carefully considered.

Extra irradiations and unexpected dose perturbations are induced by the interactions between protons and multi-leaf collimations if

[DOI: 10.18869/acadpub.ijrr.18.2.295]

we use multi-leaf collimators to form radiation fields with irregular shapes. This occurrence is an inevitable defect, and it will introduce extra doses to patients during proton therapy. Hence, many efforts must still be devoted to exploring possible ways to reduce this kind of dosimetric effect. Moreover, the long-term goal of this study is not to merely present a possible application of multi-leaf collimators in proton therapy, but it is to propose and detail a kind of beneficial mechanism for realizing proton therapy based on conformal dose layer scanning using proton radiation fields with irregular shapes. Hence, MLC collimated beams are simply a technical choice temporarily adopted by this work to investigate the dose modulation mechanism for the proposed IRF-based proton therapy. In the future, any technical solutions, e.g., fast uniform scanning technology [43], which has the potential to generate irregular proton radiation fields, could be utilized in practical applications of the proposed IRF-based proton therapy, if the dosimetric goals of clinical tumor treatments are achieved.

To facilitate the initial exploration, relatively ideal proton sources and patient geometries were adopted in this initial study. However, these factors do not hinder this work as an informative foundation for future studies of this kind. These ideal configurations and suppositions are beneficial in excluding complicated influencing factors and deriving initial research results. Further investigations for practical beam configurations and clinical tumor cases are necessary for future investigations.

CONCLUSION

Under ideal circumstances, satisfied proximal and distal dose conformities can be achieved by the proposed IRF-based proton therapy using forward radiation treatment planning and conformal dose layer stacking methods in abdominal and head anatomies. Theoretically, sharing and reusing segment shapes among different tumor slices has the potential to reduce the quantity of segment shapes and simplify radiation treatment plans for IRF-based proton therapy. Theoretically, integrating the segments with identical segment shapes and different energies into "integrated" segments has the potential to decrease the frequency of segment shape switches and improve dose delivery efficiency for IRF-based proton therapy.

ACKNOWLEDGMENTS

This work was supported in part by National Natural Science Foundation of China (Grant No. 11475087, 11605117, and 11775064); in part by the National Key Research and Development Program (Grant No. 2016YFE0103600); in part by the Project supported by the National Key Research and Development Program (Grant No. 2017YFC0107700); in part by the Postgraduate Research & Practice Innovation Program of Jiangsu Province (Grant No. KYLX16_0352); in part by the Education Department of Heilongjiang Province (Grant No. 12521425); and in part by the Priority Academic Program Development of Jiangsu Higher Education Institutions.

***Conflicts of interest*:** *Declared none.*

REFERENCES

1. Guan F, Bronk L, Titt U, Lin SH, Mirkovic D, Kerr MD, *et al*. (2015) Spatial mapping of the biologic effectiveness of scanned particle beams: towards biologically optimized particle therapy. *Sci Rep*, ***18(5):*** 9850.
2. Olsen DR, Bruland OS, Frykholm G, Norderhaug IN (2007) Proton therapy - a systematic review of clinical effectiveness. *Radiother Oncol*, ***83(2):*** 123-132.
3. Lomax AJ, Boehringer T, Coray A, Egger E, Goitein G, Grossmann M, *et al*. (2001) Intensity-modulated proton therapy: a clinical example. *Med Phys*, ***28(3):*** 317-324.
4. Brada M, Pijls-Johannesma M, De Ruysscher D (2007) Proton therapy in clinical practice: current clinical evidence. *J Clin Oncol*, ***25(8):*** 965-970.
5. Kim DW, Lim YK, Ahn SH, Shin J, Shin D, Yoon M, *et al*. 2011. Prediction of output factor, range, and spread-out Bragg peak for proton therapy. *Med Dosim*, ***36(2):*** 145-152.

[DOI: 10.18869/acadpub.ijrr.18.2.295]

6. Miyatake A and Nishio T (2013) Application of activity pencil beam algorithm using measured distribution data of positron emitter nuclei for therapeutic SOBP proton beam. *Med Phys*, ***40(9):*** 091709.
7. Zhang X, Li Y, Pan X, Li X, Radhe M, Ritsuko K, *et al*. (2009) Intensity-modulated proton therapy reduces normal tissue doses compared with intensity-modulated radiation therapy or passive scattering proton therapy and enables individualized radical radiotherapy for extensive stage IIIB non -small cell lung cancer: a virtual clinical study. *Int J Radiat Oncol Biol Phys*, ***77(2):*** 357-366.
8. Chen W, Craft D, Madden TM, Zhang K, Kooy HM, Herman GT (2010) A fast optimization algorithm for multicriteria intensity modulated proton therapy planning. *Med Phys*, ***37(9):*** 4938-4945.
9. Mailhot Vega RB, Kim J, Bussière M, Hattangadi J, Hollander A, Michalski J, *et al*. (2013) Cost-effectiveness of proton therapy compared with photon therapy in the management of pediatric Medulloblastoma. *Cancer*, ***119(24):*** 4299 -4307.
10. Iwata H, Murakami M, Demizu Y, Miyawaki D, Terashima K, Niwa Y, *et al*. (2010) High-dose proton therapy and carbon-ion therapy for stage I nonsmall cell lung cancer. *Cancer*, ***116(10):*** 2476-2485.
11. Boehling NS, Grosshans DR, Bluett JB, Palmer MT, Song X, Amos RA, *et al*. (2015) Dosimetric comparison of three-dimensional conformal proton radiotherapy, intensity-modulated proton therapy, and intensity-modulated radiotherapy for treatment of pediatric craniopharyngiomas. *Int J Radiat Oncol Biol Phys*, ***82(2):*** 643-652.
12. Chera BS, Malyapa R, Louis D, Mendenhall WM, Li Z, Lanza DC, *et al*. (2009) Proton therapy for maxillary sinus carcinoma. *Am J Clin Oncol*, ***32(3):*** 296.
13. Slater JD, Jr R, Yonemoto L, Bush DA, Jabola BR, Levy RP, *et al*. (2004) Proton therapy for prostate cancer: the initial Loma Linda University experience. *Int J Radiat Oncol Biol Phys*, ***59(2):*** 348.
14. Bussiã Re MR and Adams JA (2003) Treatment planning for conformal proton radiation therapy. *Technol Cancer Res Treat*, ***2(5):*** 389-399.
15. Zahra TK, Thomas BE, Simeon N, Jan JW, Uwe O, Karl-Axel J, *et al*. (2008) Intensity-modulated radiotherapy of nasopharyngeal carcinoma: a comparative treatment planning study of photons and protons. *Radiat Oncol*, ***24(3):*** 4.
16. Lewis GD, Holliday EB, Kocakuzel E, Hernandez M, Garden AS, Rosenthal DI, *et al*. (2016) Intensity-modulated proton therapy for nasopharyngeal carcinoma: Decreased radiation dose to normal structures and encouraging clinical outcomes. *Head Neck*, ***38(S1):*** E1886-E1895.
17. Oelfke U and Bortfeld T (2003) Optimization of physical dose distributions with hadron beams: comparing photon IMRT with IMPT. *Technol Cancer Res Treat*, ***2(5):*** 401.
18. Dinges E, Felderman N, Mcguire S, Gross B, Bhatia S, Mott S, *et al*. (2015) Bone marrow sparing in intensity modulated proton therapy for cervical cancer: Efficacy and robustness under range and setup uncertainties. *Radiother Oncol*, ***115(3):*** 373-378.
19. Wheeler A [Internet]. [cited 2015]. Available from: https://www.engineering.com/3DPrinting/3DPrintingArticles/ArticleID/9808/New-3D-Printer-Grows-Parts-from-Liquid-Its-like-the-T-1000-in-Terminator.aspx#new_tab.
20. Lin Y, Pan C, Chiang KJ, Yuan M, Chu C, Tsai YW, *et al*. (2017) Monte Carlo simulations for angular and spatial distributions in therapeutic-energy proton beams. *Radiat Phys Chem*, ***140:*** 217-224.
21. Martínez-Rovira I, Sempau J, Prezado Y (2014) Monte Carlo-based dose calculation engine for mini beam radiation therapy. *Phys Med*, ***30(1):*** 57-62.
22. Guan F, Peeler C, Bronk L, Geng C, Taleei R, Randeniya S, *et al*. (2015) Analysis of the track- and dose-averaged LET and LET spectra in proton therapy using the geant4 Monte Carlo code. *Med Phys*, ***42(11):*** 6234-6247.
23. Geng C, Moteabbed M, Seco J, Gao Y, Xu XG, Ramos-Méndez J, *et al*. (2016) Dose assessment for the fetus considering scattered and secondary radiation from photon and proton therapy when treating a brain tumor of the mother. *Phys Med Biol*, ***61(2):*** 683-695.
24. Sumini M, Isolan L, Cucchi G, Sghedoni R, Iori M (2017) A Monte Carlo model for photoneutron generation by a medical LINAC. *Radiat Phys Chem*, ***140:*** 345-348.
25. Jabbari N and Khalkhali HR (2017) Developing equations to predict surface dose and therapeutic interval in bolused electron fields: A Monte Carlo Study. *Radiat Phys Chem*, ***136:*** 64-70.
26. Peter CY, Lee CC, Chao TC, Tung CJ (2017) Monte Carlo evaluation of Acuros XB dose calculation Algorithm for intensity modulated radiation therapy of nasopharyngeal carcinoma. *Radiat Phys Chem*, ***140:*** 419-422.
27. Geng C, Tang X, Hou X, Shu D, Chen D (2014) Development of Chinese hybrid radiation adult phantoms and their application to external dosimetry. *Science China Technological Sciences*, ***57(4):*** 713-719.
28. Daartz J, Trofimov A, Paganetti H [Internet]. [cited 2009]. Available from: http://www.egms.de/static/de/meetings/ptcog2009/09ptcog047.shtml.
29. Paganetti H (2012) Proton Therapy Physics. CPC Press, New York.
30. Zhang Y, Boye D, Tanner C, Lomax A, Knopf A (2012) Respiratory liver motion estimation and its effect on scanned proton beam therapy. *Phys Med Biol*, ***57(7):*** 1779.
31. Torshabi AE (2013) Investigation of tumor motion influence on applied dose distribution in conventional proton therapy vs. IMPT; a 4D Monte Carlo simulation study. *International Journal of Radiation Research*, ***11(4):*** 225-231.
32. Grassberger C, Dowdell S, Lomax A, Sharp G, Shackleford J, Choi N, *et al*. (2013) Motion interplay as a function of patient parameters and spot size in spot scanning proton therapy for lung cancer. *Int J Radiat Oncol Biol Phys*, ***86(2):*** 380-386.
33. Paganetti H, Jiang H, Trofimov A (2005) 4D Monte Carlo simulation of proton beam scanning: modeling of variations in time and space to study the interplay between scanning pattern and time-dependent patient geometry. *Phys Med Biol*, ***50(5):*** 983-990.
34. Shinichiro M, Lei D, George S, Radhe M, Chen GTY (2014) A serial 4DCT study to quantify range variations in charged

[DOI: 10.18869/acadpub.ijrr.18.2.295]

particle radiotherapy of thoracic cancers. *J Radiat Res*, ***55 (2):*** 309-319.
35. Zenklusen SM, Pedroni E, Meer D (2010) A study on re-painting strategies for treating moderately moving targets with proton pencil beam scanning at the new Gantry 2 at PSI. *Phys Med Biol*, ***55(17):*** 5103-5121.
36. Bert C and Durante M (2011) Motion in radiotherapy: particle therapy. *Phys Med Biol*, ***56(16):*** 113-144.
37. Moorthy S, Sakr H, Hasan S, Samuel J, Al-Janahi S, Murthy N (2013) Dosimetric study of SIB-IMRT versus SIB-3DCRT for breast cancer with breath-hold gated technique. *Int J Cancer Ther Oncol*, ***1(1):*** 010110.
38. Zhang X, Guo F, Geng C, Shao W, Wang Q, Ye T, *et al*. 2014. Clinical and experimental observation of the length of time of respiratory phase: a preliminary study. *Eur Rev Med Pharmacol*, ***18(2):*** 3205-3211.
39. Eccles C, Brock KK, Bissonnette JP, Hawkins M, Dawson LA (2006) Reproducibility of liver position using active breathing coordinator for liver cancer radiotherapy. *Int J Radiat Oncol*, ***64(3):*** 751-759.
40. Du S, Zeng Z, Wu Z, Zhang K, Liu T, Chen G, *et al*. (2008) Clinical value of active breathing coordinator (ABC) during three-dimension conformal radiotherapy for patients with intrahepatic tumor. *Austral-Asian Journal of Cancer*, ***7(1):*** 15-23.
41. Frazier RC, Vicini FA, Sharpe MB, Yan D, Fayad J, Baglan KL, *et al*. (2004) Impact of breathing motion on whole breast radiotherapy: a dosimetric analysis using active breathing control. *Int J Radiat Oncol Biol Phys*, ***58(4):*** 1041-1047.
42. Remouchamps VM, Vicini FA, Sharpe MB, Kestin LL, Martinez AA, Wong JW (2003) Significant reductions in heart and lung doses using deep inspiration breath hold with active breathing control and intensity-modulated radiation therapy for patients treated with locoregional breast irradiation. *Int J Radiat Oncol Biol Phys*, ***55(2):*** 392-406.
43. Zenklusen SM, Pedroni E, Meer D, Bula C, Safai S (2011) Preliminary investigations for the option to use fast uniform scanning with compensators on a gantry designed for IMPT. *Med Phys*, ***38(9):*** 5208.

[DOI: 10.18869/acadpub.ijrr.18.2.295]